Engineering xxx (xxxx) xxx

Contents lists available at ScienceDirect

Engineering

journal homepage: www.elsevier.com/locate/eng

Research
Food Science and Engineering—Article

Single-cell RNA sequencing reveals 7-ketositosterol exacerbates aortic inflammation through TLR4 signaling-regulated IRF5 mediated M1 macrophage polarization

Qinjun Zhang [a], Weisu Huang [a], Cheng Chen [b], Jianfu Shen [a], Baiyi Lu [a,*], Peiwu Li [c]

[a] College of Biosystems Engineering and Food Science, National-Local Joint Engineering Laboratory of Intelligent Food Technology and Equipment, Key Laboratory for Agro-Products Nutritional Evaluation of the Ministry of Agriculture and Rural Affairs, Zhejiang University, Hangzhou 310058, China
[b] Center for Ultrasound Molecular Imaging and Therapeutics, University of Pittsburgh, Pittsburgh, PA 15260, USA
[c] Oil Crops Research Institute, Chinese Academy of Agricultural Sciences, Wuhan 430062, China

ARTICLE INFO

Article history:
Received 31 May 2024
Revised 30 April 2025
Accepted 21 July 2025

Keywords:
Single-cell analysis
7-ketositosterol
Macrophage
Inflammation
Polarization

ABSTRACT

Atherosclerosis (AS) is a chronic inflammatory disease in which macrophages play an indispensable role. Exploration of the effects of aortic cell subpopulations in AS remains challenging due to cellular heterogeneity. Phytosterol oxidation products (POPs) are key dietary factors influencing AS due to their potential pro-inflammatory effects in atherosclerotic mice. However, the contribution of alterations in cellular heterogeneity to this outcome and the exact mechanisms remain elusive. Here, we constructed a novel single-cell transcriptomic landscape of arteries in ApoE$^{-/-}$ mice fed an atherosclerotic diet without or with POPs. Combining single-cell RNA sequencing (scRNA-seq) with *in vitro* functional validation, we demonstrated that 7-ketositosterol, a major component of POPs, induced macrophages to skew the pro-inflammatory (M1) phenotype through the TLR4-IRF5 axis, thereby amplifying the inflammatory response. Notably, we verified the presence of this pro-inflammatory immune niche with the same molecular features using publicly available human arterial scRNA-seq data. This demonstrates that this is a reproducible characteristic in human AS. Our study shifts the current paradigm of exploring the biological effects of food components, and provides unprecedented perspectives for the application of single-cell technology to food nutrition research.

1. Introduction

Atherosclerosis (AS), a chronic inflammatory disease, constitutes the principal underlying etiology of cardiovascular diseases worldwide [1]. It is characterized by plaque buildup in the arteries, leading to thickened arterial walls, reduced elasticity, and narrowing of the arterial lumen. The advancement of arterial plaques is characterized by endothelial layer impairment, oxidized low (ox)-density lipoprotein (LDL) deposition in the intimal space, increased macrophage recruitment, and fibrous connective tissue proliferation [2]. Recent phase III clinical trials have supplied evidence supporting the notion that a focus on inflammation may improve cardiovascular outcomes, underscoring its pivotal role in atherogenesis [3,4].

The intricate cellular composition of human AS and its connection to disease progression and clinical complications have yet to be determined. Vascular tissues display notable diversity influenced by hemodynamic conditions, cellular origin, recruitment, and trans-differentiation processes. A variety of immune cells reside within the arterial wall, with macrophages predominating within AS plaques. Polarization of macrophages disrupts inflammatory homeostasis, which mechanistically governs the onset, progression, and eventual plaque rupture in AS. Depending on their roles in AS, macrophages are divided into anti-inflammatory (M2) and pro-inflammatory (M1) types. However, there is a growing argument that the heterogeneity of macrophages within plaques cannot be adequately explained solely by the traditional M1–M2 macrophage polarization paradigm, particularly with the advancement of single-cell technology. Conventional methods are insufficient for capturing the intricate cellular architecture inherent in AS. As observed in recent single-cell evidence of atherosclerotic plaques from humans [5] and mice [6,7], three main macrophage

* Corresponding author.
E-mail address: bylu@zju.edu.cn (B. Lu).

https://doi.org/10.1016/j.eng.2025.07.021

Please cite this article as: Q. Zhang, W. Huang, C. Chen et al., Single-cell RNA sequencing reveals 7-ketositosterol exacerbates aortic inflammation through TLR4 signaling-regulated IRF5 mediated M1 macrophage polarization, Engineering, https://doi.org/10.1016/j.eng.2025.07.021

populations with varying inflammatory characteristics have been delineated. Therefore, it can be concluded that recent breakthroughs in single-cell molecular profiling have enabled unprecedented resolution in cellular characterization. This has resulted in breakthroughs in our understanding of the cellular biodiversity within atherosclerotic plaques.

Numerous risk factors, including elevated cholesterol, low levels of high-density lipoprotein, obesity, hypertension, diabetes mellitus, inactive lifestyle, and an unhealthy diet, are linked to the initiation, progression, and outcomes of AS. Cholesterol-rich diets are known for their role in elevating blood cholesterol levels, consequently hastening the progression of AS by fostering the accumulation of lipids and macrophages within arterial plaques.

In addition to cholesterol, diet-derived sterols and their derivatives, including sterol oxidation product (POP) and phytosterol (PS), significantly influence AS progression [8,9]. PS derived from plants shares structural similarities with cholesterol but differs in its side chains. Research demonstrates that consuming 2–3 g of PS daily decreases LDL cholesterol concentrations by as much as 12% [10]. However, similar to other unsaturated dietary constituents, PS are susceptible to oxidation under processing conditions (e.g., frying and heating), leading to the formation of POPs [11]. Oxidation of PS not only diminishes its cholesterol-lowering properties but is also thought to promote AS [12], potentially attributed to elevated circulatory levels of oxidized PS detected in AS patients [13]. In addition to their pro-atherosclerotic effects, POPs also induce cytotoxicity [14–16], apoptosis [17], disrupt intestinal cholesterol metabolism [18], and exhibit proinflammatory properties [19–21]. The majority of POPs in humans originate from dietary sources, with 7-ketositosterol (7-KS) being quantitatively the most prevalent POP in food. A recent study found that 7-KS in ultra-processed foods exacerbated colitis in mice through modulating the gut microbiota [20]. Although the cellular heterogeneity of atherosclerotic plaques is gradually being revealed, studies focused on the effects of diet or dietary components on aortic cellular heterogeneity and the development of AS remain scarce. Moreover, the impact of POPs on aortic cell heterogeneity and immune cell subpopulations, and the subsequent effect on pro-atherosclerotic mechanisms, has not yet been reported.

To fill these research gaps, we performed an in-depth analysis of single-cell transcriptomic data derived from the aortas of ApoE$^{-/-}$ mice administered control (Con) or POP-supplemented diets. Herein, we constructed a detailed reference map delineating the cellular composition within mouse atherosclerotic plaques. Importantly, our single-cell data revealed an M1-like macrophage transcriptional state suggestive of cellular disease. We also determined that Toll-like receptor (TLR) signaling and the transcription factor IRF5 exerted a pivotal influence on the induction of M1-like macrophages in the POP group. Further experimental verification revealed that in ox-LDL stimulated bone marrow-derived macrophage (BMDM) and RAW 264.7 cells, the proinflammatory effects and M1 polarization induced by 7-KS were dependent on the TLR4–IRF5 axis. Further, we found that M1 polarization and pro-inflammatory effects of 7-KS were largely abolished after treatment with TLR4 and IRF5 inhibitors. Concurrently, by comparing publicly accessible single-cell transcriptomic data from human normal arteries and advanced carotid plaques, we recognized the widespread presence of the pro-inflammatory immune niche exhibiting the molecular features associated with POP, suggesting a reproducible feature of this pathogenic immune niche in human AS. Overall, these results elucidate the pathogenic cellular features and molecular events underlying POP's pro-inflammatory effects. This suggests new avenues for the application of single-cell RNA sequencing (scRNA-seq) technologies for determining the biological impacts of dietary components at the single-cell level, and may be used to determine potential therapeutic strategies for the treatment of AS.

2. Methods

2.1. scRNA-seq data and analysis

ScRNA-seq was performed on aortic tissues from male ApoE$^{-/-}$ mice fed a pro-atherosclerotic diet (60% energy from fat; 0.2% cholesterol) with or without 0.02% POPs for 14 weeks. Table S1 in Appendix A shows the composition of the phytosterol oxidation products in the POP diet (mg·kg^{-1}). The scRNA-seq was performed following the 10 × Genomics protocol (LC-Bio Technology Co., Ltd., China). Sample demultiplexing, barcode identification, and 3′ gene counting were conducted using the Cell Ranger software (version 3.1.0, USA). The GRCh38/GRCm38 ensemble genome was used as the reference genome. ScRNA-seq data were analyzed with Seurat (version 3.1.1, USA) for dimensional reduction, clustering, and analysis. The number of genes expressed in each cell ranged from 500 to 5000, and unique molecular identifier (UMI) counts were less than 500. Mitochondrial gene expression accounted for <10% of total reads. Seurat was applied for dimensionality reduction and t-distributed stochastic neighbor embedding (t-SNE)-based (two-dimensional) 2D visualization. Marker gene identification was achieved through Seurat's FindAllMarkers algorithm. Enrichment analysis, Gene Ontology (GO) enrichment analysis, cell–cell interaction analysis, pseudo-time trajectory analysis, RNA velocity analysis, and other bioinformatics analyses were performed with the OmicStudio tools (China).

2.2. Cell culture

To obtain bone marrow-derived macrophages (BMDMs), mice aged 6–8 weeks (C57BL/6J background) were killed, and the tibiae and femurs were harvested. Bone marrow cells were flushed out using ice-cold PBS and filtered through a 70 μm cell strainer to eliminate debris. After centrifugation of the filtered suspension at 500 × *g* (*g*: centrifugal force; 5 min, 4 °C), the supernatant was removed, and the pellet was treated with pre-chilled RBC lysis buffer. Cells were then maintained in complete dulbecco's modified eagle's medium (DMEM) medium containing 20 ng·mL^{-1} macrophage-colony stimulating factor (MCSF). Subsequent experiments were conducted after 7 days to ensure the full differentiation of BMDMs. RAW264.7 cells were cultured in high-glucose DMEM containing 1% antibiotic–antimycotic solution and 10% fetal bovine serum (FBS).

2.3. Cell viability assay

BMDM cell viability in different groups was evaluated via the cell counting Kit-8 assay. BMDM (8×10^3 cells/well) were plated in 96-well plates. Cells were cultured for 24 h in medium supplemented with graded concentrations of 7-KS. Subsequently, the culture medium was substituted with 100 μL of fresh medium supplemented with 10 μL CCK-8 (40203ES76, Yeasen, China). Following a 1 h incubation, the 450 nm absorbance was assessed.

2.4. Western blotting

Total cellular proteins were isolated with RIPA Lysis Buffer (Beyotime, Cat# P0013C, China). Nuclear protein was isolated using the Nuclear Protein Extraction Kit (R0059, Solarbio, China). The BCA Protein Assay Kit (PC0020, Solarbio, China) was utilized to determine the concentration of isolated proteins. Equal amounts of protein (15 μL per lane) were loaded onto 6%–15% sodium dode-

cyl sulfate–polyacrylamide gel electrophoresis (SDS-PAGE) gels, subjected to electrophoresis, and transferred onto polyvinylidene fluoride (PVDF) membranes. After blocking with 5% skim milk in tris buffered saline with tween-20 (TBST), membranes were probed with primary antibodies overnight at 4 °C, followed by incubation with species-matched horseradish peroxidase-conjugated secondary antibodies (1:10000) for 2 h. Subsequently, target protein signals were detected with enhanced chemiluminescence (ECL) chemiluminescent substrate. The relative band intensities were normalized to glyceraldehyde-3-phosphate dehydrogenase (GAPDH), α-tubulin, and Lamin A. Table S2 in Appendix A shows specific antibody information used. Quantification of immunoblot data was conducted via Clinx Image Analysis software (China).

2.5. Quantitative real-time polymerase chain reaction (qRT-PCR)

Total RNA from macrophages was isolated using an RNA Extraction Kit (AC0202-A, SparkJade, China). The complementary deoxyribonucleic acid (cDNA) synthesis reaction mixture consisted of 1 μg of template RNA. The reaction was carried out following the provided instructions (AG0304-B, SparkJade, China). SYBR Green PCR Mix Kit (AH0104-B, SparkJade, China) was used to detect target gene content. Relative mRNA levels were determined via the $2^{-\Delta\Delta CT}$ (CT, cycle threshold) method Cycle Threshold and normalized to endogenous *Gapdh* levels. Primer sequences are shown in Table S3 in Appendix A.

2.6. Enzyme-linked immunosorbent assay (ELISA)

BMDM and RAW264.7 cells were seeded on 6-well plates. The cells were treated with varying concentrations of 7-KS and 90 $\mu g \cdot ml^{-1}$ ox-LDL (Yiyuan Biotechnology, China) for 24 h. After treatment, culture supernatants were harvested through centrifugation. The concentrations of bioactive cytokines (IL-6, TNF-α, IL-10, and IL-6) were determined with commercial ELISA kits (Meimian, China).

2.7. Immunofluorescence

Cell samples were treated with 4% paraformaldehyde and then incubated with 0.05 % Triton X-100 solution for 15 min. Slides were then blocked with blocking solution (Beyotime, China), incubated with primary antibodies at 4 °C overnight. Subsequently, slides were incubated for 1 h with fluorescently labeled secondary antibodies and 4′,6-diamidino-2-phenylindole (DAPI) solution. Staining was observed under a fluorescence microscope. Three biological repeats were conducted.

2.8. Verification in the human community-available scRNA-seq datasets

Human scRNA-seq datasets comparing atherosclerotic and normal arterial tissues were retrieved from the Gene Expression Omnibus (USA). Six normal ascending aorta (AA) samples (GSE216860) and three AA specimens (GSE213740) were sourced from the GEO databases to provide non-atherosclerotic arteries [22]. Atherosclerotic carotid arteries included six samples (GSE210152) [23] and 4 samples (GSE234077) [24]. Stringent quality control thresholds were applied, retaining cells expressing 200–5000 genes with mitochondrial content under 25% for subsequent analysis. To mitigate batch effects, we applied the harmony algorithm. Classification of cell types in precomputed clusters was performed based on previously reported markers. GO analysis, kyoto encyclopedia of genes and genomes (KEGG) analysis, gene set enrichment analysis (GSEA) analysis, and single-cell regulatory network inference and clustering (SCENIC) were used to identify cell type-specific pathways and potential transcriptional regulators between normal and atherosclerotic tissues.

2.9. Statistics

Statistical analysis was performed using R (V 4.3.2) and GraphPad Prism (V 9.5). All results are expressed as the mean ± standard error of the mean (SEM). One-way analysis of variance (ANOVA) was employed to assess distinctions between multiple groups. Dunnett's *post hoc* test was used for pairwise comparisons. Significance levels were established at $^{*}P < 0.05$, $^{**}P < 0.01$, and $^{***}P < 0.001$, with NS indicating no statistical significance.

3. Results

3.1. Single-cell atlas and characterization of cellular heterogeneity in $ApoE^{-/-}$ mouse aorta plaques

To explore the effect of POPs on the overall heterogeneous characterization of aortic cells, we performed scRNA-seq on single cells collected from $ApoE^{-/-}$ mice consuming high fat POP-riched diets (Fig. 1(a)). After quality control and filtering, 2996 and 3914 cells from the aortas of the Con and POP groups, respectively, were used for downstream analysis. Fig. 1(b) (right) revealed a difference in the overall cell atlas between the Con and POP mouse aortas. Unsupervised clustering with t-SNE annotated 20 sub-cell clusters (Fig. 1(b)). Based on identified cellular markers and highly expressed signature genes in each population (Table S4 in Appendix A), these cell populations in the aortas were stratified into five subtypes, namely fibroblast cells (marked by *Serpinf1*, *Pi16,* and *Pdgfa*), myeloid cells (marked by *Adgre1*, *Ccr2*, *Itgax*, *Cd14*, *Cd68*, *Csf1r*, and *Lgals3*), lymphocytes (marked by *Cd3d*, *Cd79a*, *Cd8b1*, and *Nkg7*), smooth muscle cells (SMCs) (marked by *Acta2*, *Myh11*, and *Tagln*), and endothelial cells (marked by *Pecam1*, *Ptprb*, *Cdh5,* and *Fabp4*) (Figs. 1(b) and (c)) [25,26]. The heatmap displayed the top 10 genes exhibiting high expression levels within each cluster (Fig. 1(d)). To analyze differences in the cell microenvironment between the Con and POP groups, variations in cellular composition were compared between the two groups. Results showed an increase in the number of lymphocytes (from 9.72% to 16.40%) and SMCs (from 3.70% to 3.99%), and a decrease in the number of endothelial cells (from 6.29% to 2.81%), fibroblast cells (from 63.13% to 61.91%), and myeloid cells (from 17.15% to 14.90%) in the POP-treated group (Figs. 1(e) and (f)). The proportions of five major cell types and differentially expressed genes between the Con and POP groups indicated that POP treatment changed the number and gene expression of aortic cell subsets (Fig. 1(e) and Fig. S1(a) in Appendix A).

To investigate whether POP treatment resulted in changes in intercellular communication, we computed the integrated cell–cell interaction networks by analyzing the quantity and intensity of interactions in the Con and POP groups. A significant reduction in both interaction number and intensity between lymphocytes and other cells was observed in the POP group compared to the Con group (Fig. 1(g), Figs. S1(b) and (c) in Appendix A). Notably, the number of myeloid cells interacting with myeloid cells, SMCs, and endothelial cells increased significantly after POP treatment, while the number of interactions with lymphocytes decreased significantly (Fig. 1(g)). Additionally, the cell–cell interactions between myeloid cells and other cells (including lymphocytes, SMCs, and endothelial cells) in the POP group were markedly strengthened (Fig. 1(h)). This finding indicated that myeloid cells may assist in orchestrating the recruitment of other cells in the plaque microenvironment. Therefore, we further conducted map-

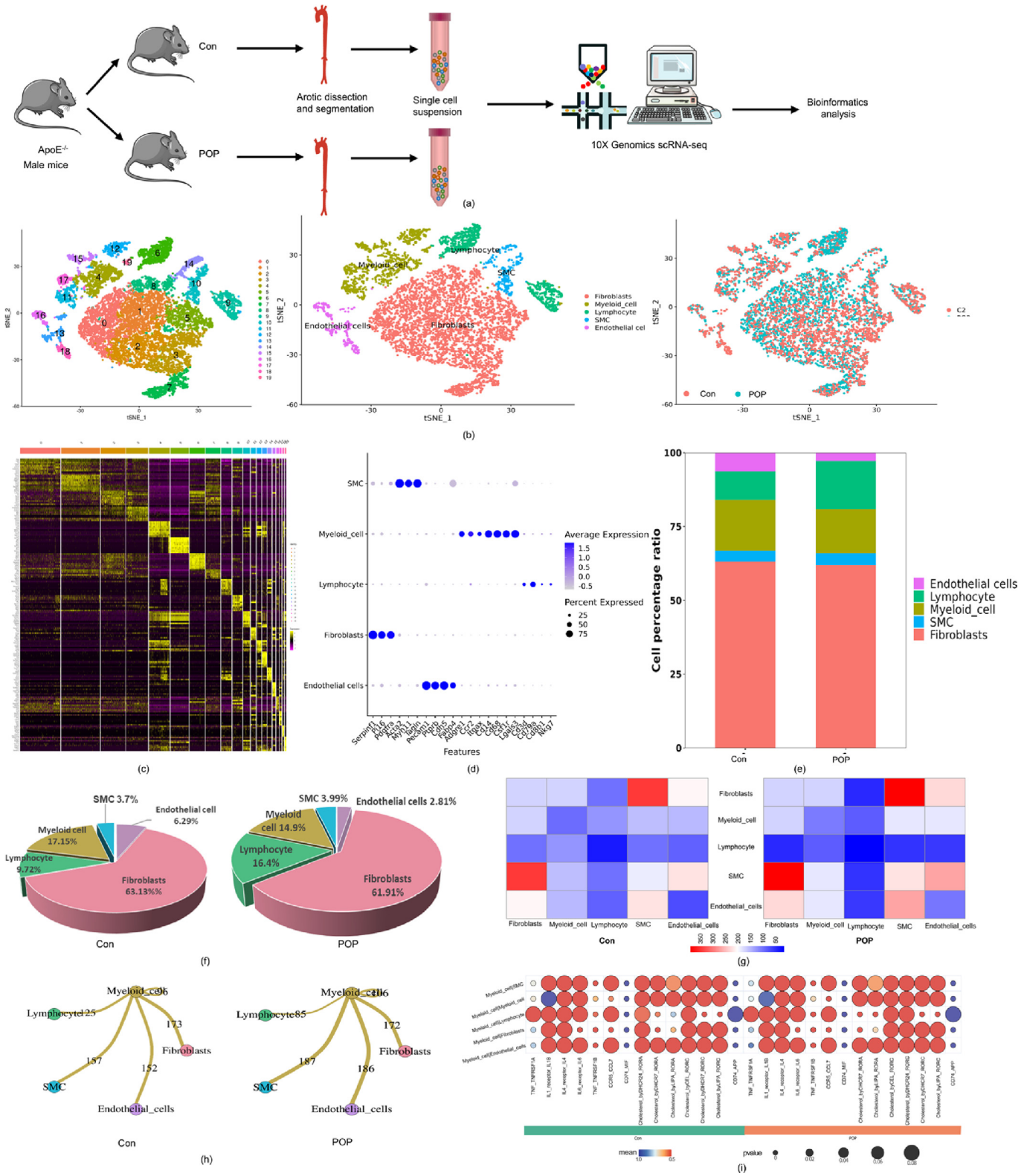

Fig. 1. scRNA-seq analysis revealed that POP altered aortic cell heterogeneity. (a) Workflow for single-cell RNA transcriptome experiments. (b) T-SNE visualization displayed 20 minor (left) and five major clusters (middle) in two groups (right). (c) Dot plot of 5 major cell markers. (d) Heatmap of differentially expressed genes in each subpopulation. The proportions of major clusters in the Con and POP groups were shown in a stacked bar plot (e) and a 3D pie chart (f). (g) Ligand–receptor pair numbers per cell type in Con and POP groups. (h) Interaction intensity between myeloid cell and other cell types in the Con and POP groups. (i) Bubble chart depicting markedly elevated ligand–receptor interactions between source and target cells, color-coded by experimental group. The selected ligand–receptor pairs orchestrating myeloid-to-nonmyeloid cellular crosstalk in the Con and POP groups.

ping of ligand-receptor pairs within myeloid cell populations (Fig. 1(i)). The interaction of TNF-TNFRSF1A, a key regulator of inflammation, with myeloid cells and endothelial cells, fibroblasts, myeloid cells, and SMCs was enhanced. This indicated that POP treatment promoted myeloid cell-mediated inflammation [27]. Collectively, these findings revealed that POP treatment notably changed aortic cell heterogeneity and cell–cell interactions in the microenvironment. This also suggests myeloid cells potentially serve as a key determinant of the effect of POP-induced inflammation due to their integral role as immune cells in AS onset and progression. Therefore, we further focused on myeloid cell subsets in our follow-up analyses to investigate their contribution to the proinflammatory effects of POP.

3.2. Association of M1-like macrophages with aortic inflammation

Given the observed changes in the myeloid cell compartment following POP treatment, unsupervised clustering was performed on myeloid populations to explore cellular heterogeneity. Four myeloid cell subclusters were identified based on gene expression (Figs. 2(a)–(c); Table S5 in Appendix A). Tissue-resident like macrophages were characterized based on the levels of *F13a1* and *Lyve1*, which are classical markers of resident-like macrophages [28]. Monocytes highly expressed *Ly6c2* and *Ccr2*, which resemble the classical monocyte signature [29]. Antigen-presentation macrophages displayed relatively high *H2-Ab1*, *H2-Aa*, and *H2-Eb1* expression levels, hallmark genes for antigen presentation [30]. M1-like macrophages were enriched in *Nlrp3*, *Nfkbid*, *Tnf*, and *Ccl3*, which are known markers of pathological pro-inflammatory cells [31]. Next, we compared changes in the relative proportion of the four subpopulations after POP treatment. Notably, the levels of antigen-presentation macrophages, M1-like macrophages, and monocytes were remarkably elevated after POP treatment. Meanwhile, Res-like macrophages gradually reduced (Fig. 2(d)). Cell–cell interaction analysis revealed that POP decreased communication between M1-like macrophages and monocytes, and enhanced communication between antigen-presenting cells and M1-like macrophages (Fig. S2(a) in Appendix A). To determine the potential relationships between the subpopulations of myeloid cells, we explored the dynamic immune status and transformation of subpopulations of myeloid cells using the pseudotime analysis. We noted that monocytes were positioned at the start of the pseudotime trajectory, while antigen-presentation macrophages, M1-like macrophages, and tissue-resident like macrophages were at the end of the trajectory (Fig. 2(e)). Tracking of changes in gene expression between the monocyte–macrophage compartments identified differentiation trajectories that specify functional identities of macrophage subgroups. Based on reconstructed pseudotime trajectories, we tracked significantly relevant genes involved in navigating the decision over pseudotime. The antigen-presentation macrophage branch exclusively expressed antigen-presenting genes (*H2–Ab1*, *H2–Eb1*, and *H2–Aa*). The M1-like macrophage branch began to express canonical genes related to macrophage polarization, proinflammatory genes such as *Nlrp3*, *Tlr4*, *Tnf*, and *Ccl7*, and genes related to lipid metabolism (*Apoe* and *Abca1*; Fig. 2(f)).

We then conducted RNA velocity analysis to elucidate the cellular response of myeloid cells to aortic inflammation. This analysis allows estimation of dynamic timescales of gene expression state by examining spliced and unspliced messenger ribonucleic acid (mRNA) [32]. RNA velocity trajectories aligned with pseudo-time analysis results, revealing a shift between monocytes and M1-like macrophages in the inferred future state, indicating the existence of a dynamic process between these two subpopulations (Fig. 2(g)). We further attempted to delve into identifying dynamic driver genes under the fate of monocyte and M1-like macrophages. Interestingly, we found that the top-ranked dynamic driver genes for M1-like macrophages and monocytes were *Il1r1* and *Irf4*, respectively (Fig. 2(h) and Fig. S2(b) in Appendix A). Il1r1 (interleukin-1 receptor 1) is a major binding site for cytokines of interleukin-1 family, which is a pivotal inflammatory mediator involved in a variety of immune responses and pathological processes. The results suggest that inflammation may influence macrophage M1 polarization. The interferon regulatory factor 4 (IRF4) functions as a transcriptional modulator of interferon signaling pathways. IRF4 regulates multiple immune system processes, especially in regulating the development and function of immune cells. These findings illustrate the critical involvement of M1-like macrophages in the secretion of pro-inflammatory factors, which thereby trigger an inflammatory response during the aortic inflammation.

3.3. Identification of specific signaling pathways and regulators of M1-like macrophages

Next, we investigated the functional characteristics of M1-like macrophages during aortic inflammation. GO enrichment analysis revealed that differentially expressed genes (DEGs) in M1-like macrophages were associated with the immune response, positive regulation of the inflammatory response, LDL particle receptor activity, macrophage cytokine production, and toll-like receptor 4 (TLR4) signaling pathway (Fig. 3(a)). Interestingly, TLR4 has been reported to recognize modified lipoproteins [33]. This observation was further confirmed by GSEA. It is noteworthy that M1-like macrophages in the POP group were characterized by the inflammatory response and toll-like receptor signaling (Fig. 3(b)). This illustrates the augmented M1-like macrophage inflammatory response in the POP group.

To delve into the phenotype of POP-treated M1-like macrophages, we scored the set of genes of interest. We then computed toll-like receptor signaling pathway and inflammatory response gene-set scores in the Con and POP groups. This analysis further confirmed that both gene set scores in POP-treated macrophages were higher than in the Con group, suggesting that POP shifted macrophages toward an inflammatory state (Fig. 3(c)). Sample-specific gene regulatory networks were constructed using pySCENIC to identify transcriptional controllers of M1-like macrophages through co-expression analysis. We examined representative transcription factor regulons in M1-like macrophages. Top-ranked M1-like macrophage regulons (sorted by specificity metrics) are prominently highlighted in the scatter plot, with maximal activity clusters distinctly visualized (Fig. S3 in Appendix A). Further, we focused on the activity of transcription factors associated with polarization, the inflammatory response, and metabolism in macrophages [31,34]. The results of the regulons-opening heatmap are shown in Fig. 3(d). Of note, there was an increase in the number of cells with IRF5 transcription factors in the open state after POP treatment (Fig. 3(d)). Concurrently, the mapped area under the curve (AUC) values of IRF5 transcription factors also showed high expression in M1-like macrophages (Fig. 3(e)). IRF5 belongs to the interferon regulatory factor family. Interestingly, a strong association between IRF5 and TLRs has been extensively reported. TLR4 signaling enhances IRF5-mediated transcriptional activation of target genes, a process required for systemic sclerosis progression [35]. In addition, the dot plot demonstrated that heightened expression of inflammation-related genes in M1-like macrophages, consistent with their characteristic pro-inflammatory function (Fig. 3(f)). This suggests that POP amplified the pro-inflammatory activity of M1-like macrophages, contributing to enhanced aortic inflammation during AS development. These profound variations underscore the pronounced inflammatory response in M1-like macrophages and highlight the dominant role of the TLR4 signaling

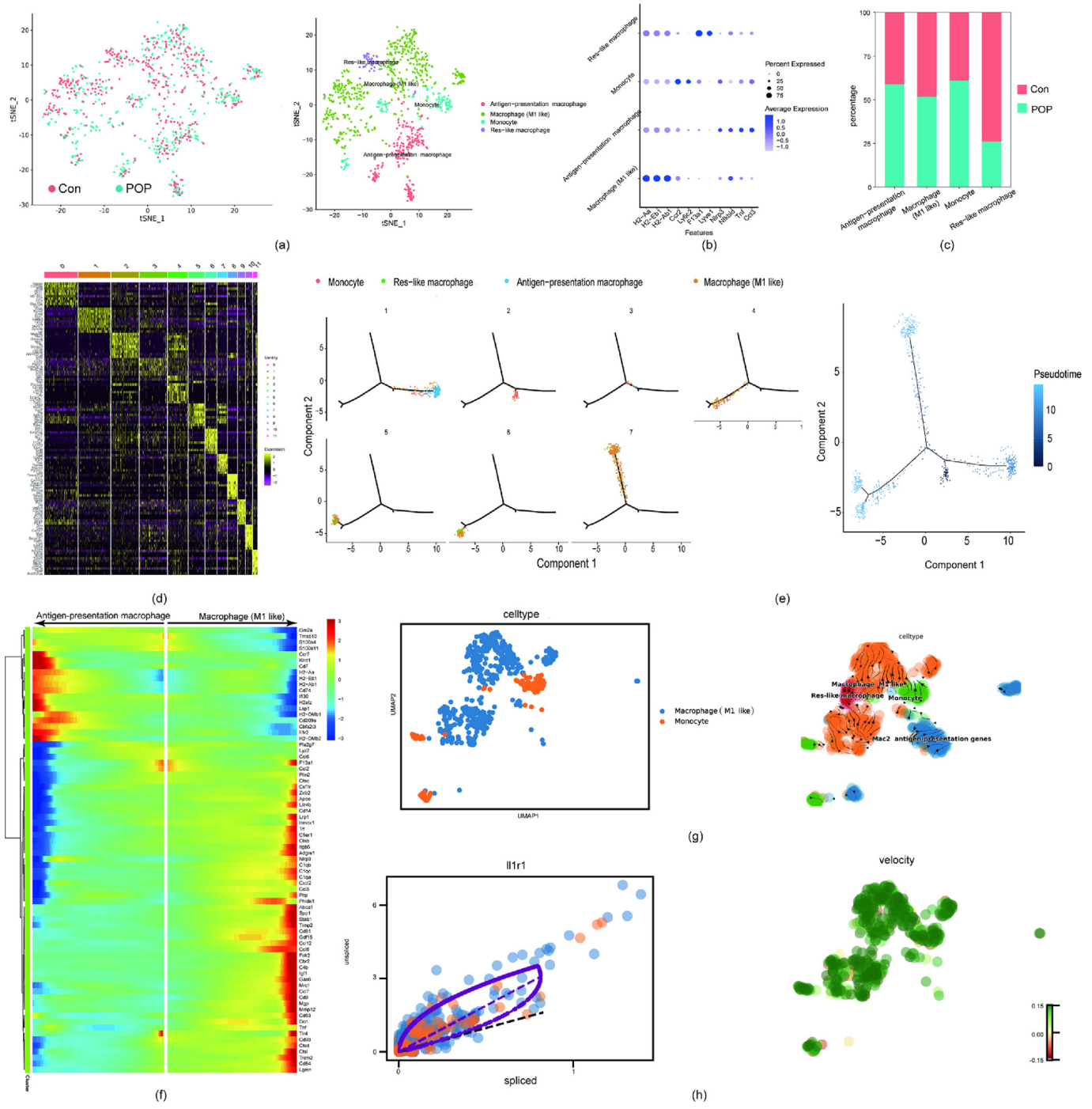

Fig. 2. POP reshaped the composition of myeloid cells. (a) The t-SNE projection of myeloid subsets across the Con and POP groups. (b) The representative top marker genes in myeloid subsets. (c) Heatmap depicting marker gene expression profiles across myeloid subtypes. (d) The number of macrophage subpopulations in the Con and POP groups. (e) Macrophage trajectory analysis by subtype (left) and pseudo-time (right). (f) Heatmap depicting scaled expression of branching curated genes of antigen-presentation macrophage and M1-like macrophage fates ordered by pseudotime. (g) The relationship between monocyte and M1-like macrophage clusters was analyzed with RNA-velocity. Uniform manifold approximation and projection (UMAP) arrows represent the orientation of anticipated transcriptional dynamics in cells. (h) Gene expression and splicing rate of the top 1 rank velocity in M1-like macrophages.

pathway and IRF5 transcription factor in mediating the inflammatory response of macrophages. It was thus proposed that IRF5 may serve as a key downstream mediator of POP, which affects aortic inflammation through the TLR4 signaling pathway.

3.4. 7-KS promoted pro-inflammatory macrophage M1 polarization

An *in vitro* stimulation assay utilizing BMDMs was conducted to validate the capacity of candidate factors to facilitate plaque-associated macrophage phenotypic modulation. Due to the characteristic accumulation of ox-LDL in the subendothelial layer in AS arteries, ox-LDL was employed to simulate the atherosclerotic plaque environment. The regulatory effect of 7-KS on macrophage viability was initially assessed under *in vitro* conditions. Our findings revealed 7-KS treatment had no effect on BMDM viability (Fig. S4 (a) in Appendix A). Subsequently, the contribution of 7-KS in the macrophage inflammatory response and polarization after ox-LDL stimulation *in vitro* was systematically examined. The production

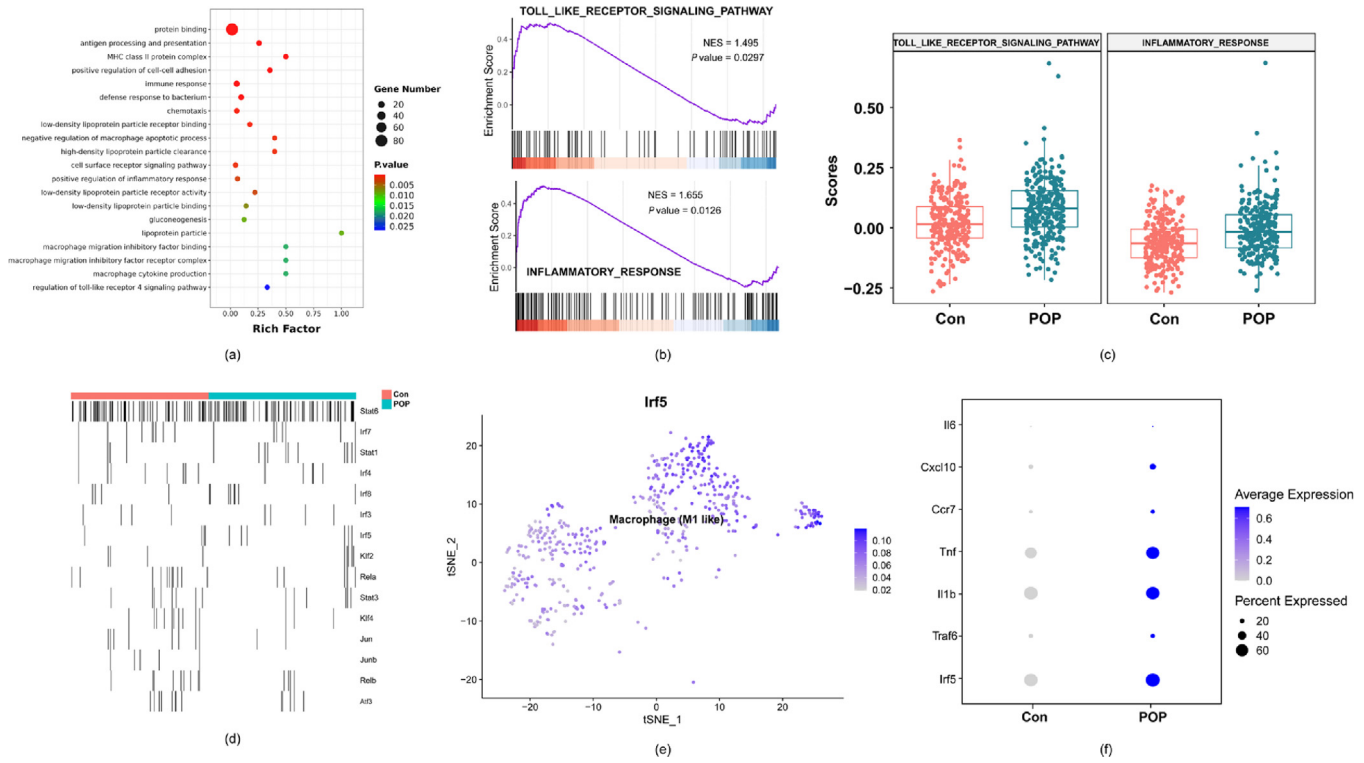

Fig. 3. Identified distinct regulators governing macrophage subset identity maintenance. (a) The selected 20 GO-annotated biological processes linked to M1-like macrophage DEG upregulation. (b) Enriched hallmarks of the toll-like receptor signaling pathway and the inflammatory response between the Con and POP group as determined via GSEA. (c) Toll-like signaling pathway and inflammatory response scores in the Con and POP group were computed using the *AddModuleScore* function and visualized via box plot. (d) Regulons open heatmap. Rows represent regulons, while columns indicate cells. The black in the figure indicates "ON" (i.e., the regulon is in an active and open state in the cell); white in the figure indicates "off" (i.e., the regulon is in the active off state in that cell). (e) T-SNE showing the M1-like macrophages with high expression of IRF5 in the Con and POP groups. (f) The inflammation-associated genes within M1-like macrophages across both experimental groups.

of TNF-α, Il-1β, and Il-6 by ox-LDL-treated macrophages was significantly increased, indicating that inflammation occurred in these macrophages. Surprisingly, 20 μmol·L^{-1} 7-KS treatment exacerbated the secretion of these inflammatory factors (Fig. 4(a)). Moreover, 4 μmol·L^{-1} 7-KS also markedly elevated IL-6 levels (Fig. 4(a)). In agreement with the inflammatory cytokine secretion findings, 20 μmol·L^{-1} 7-KS treatment markedly elevated TNF-α protein levels (Fig. 4(b)). Conversely, 7-KS had no significant effect on IL-10 secretion levels (Fig. S4(b) in Appendix A), indicating that 7-KS had no effect on anti-inflammatory factors. INOS is a marker of M1 macrophages. We detected the number of M1 macrophages by immunofluorescence and observed that 7-KS treatment increased the number of iNOS^{+} macrophages (Fig. 4(c)). We also evaluated whether the pro-inflammatory effects of 7-KS were specific to BMDM or a general phenomenon associated with other types of macrophages. Consistent with the BMDM results, ox-LDL treatment induced a significant increase in proinflammatory factor secretion, and 20 μmol·L^{-1} 7-KS exerted a potent pro-inflammatory effect in ox-LDL-stimulated RAW264.7 macrophages through facilitating IL-6, TNF-α, and IL-1βsecretion (Fig. 4(d)). Interestingly, 4 μmol·L^{-1} 7-KS significantly increased TNF-α levels, which was different from the effect of the same concentration on BMDM. Additionally, no significant modulation of IL-10 release was detected in 7-KS-exposed conditions (Fig. S4(c) in Appendix A). We also found that 7-KS treatment significantly enhanced *CD86* mRNA expression, a marker gene associated with M1 macrophages (Fig. 4(e)). Immunofluorescence quantification of the expression of CD86 demonstrated that ox-LDL treatment increased the CD86 proteins, while this effect was aggravated by 7-KS (Fig. 4(f)). In addition, no marked changes were detected in gene expression levels associated with macrophage activation to the M2 type (*Arg1*) in BMDM and RAW 264.7 cells (Figs. S4(d) and (e) in Appendix A). Taken together, these data show that 7-KS exerts a pro-inflammatory effect and skews macrophages toward the M1 type in ox-LDL-activated macrophages *in vitro*.

3.5. 7-KS upregulated M1-Skewing in a TLR4/IRF5-Dependent Manner

The scRNA-seq analysis revealed that the TLR4 signaling pathway and the transcription factor IRF5 were prominently enriched in M1-like macrophages after POP treatment. Prior research has suggested that IRF5 acts as a pivotal transcription factor in the TLR4-MyD88-dependent signaling pathway, facilitating the activation of proinflammatory cytokines [36]. Therefore, we analyzed the activation of TLR4-IRF5 signaling under ox-LDL stimulation conditions in BMDM and RAW264.7 cells (Fig. 5). Of note, the expression of TLR4-IRF5 signaling pathway related proteins (TLR4, Myd88, and TRAF6) was significantly increased in BMDM and RAW 264.7 cells after 7-KS treatment (Figs. 5(a) and (d)). Consistent with this, 7-KS treatment also significantly increased the mRNA levels of *Tlr4*, *Myd88*, and *Traf6* in ox-LDL-induced RAW 264.7 macrophages (Fig. S5 in Appendix A). Stimulation of TLRs triggers a series of IRF5 phosphorylation events, promoting its nuclear translocation and subsequently driving the expression of inflammatory cytokine genes [37]. Therefore, we investigated whether nuclear translocation of IRF5 occurred in BMDM and RAW 264.7 cells stimulated by ox-LDL. Experimental findings revealed that ox-LDL notably increased IRF5 nuclear translocation, and this effect was further profoundly strengthened by 7-KS (Figs. 5(b) and (e)), which explains the pro-inflammatory effect of 7-KS. Overall, our data suggest that 7-KS regulates M1-macrophages skewing through the TLR4–IRF5 signaling pathway.

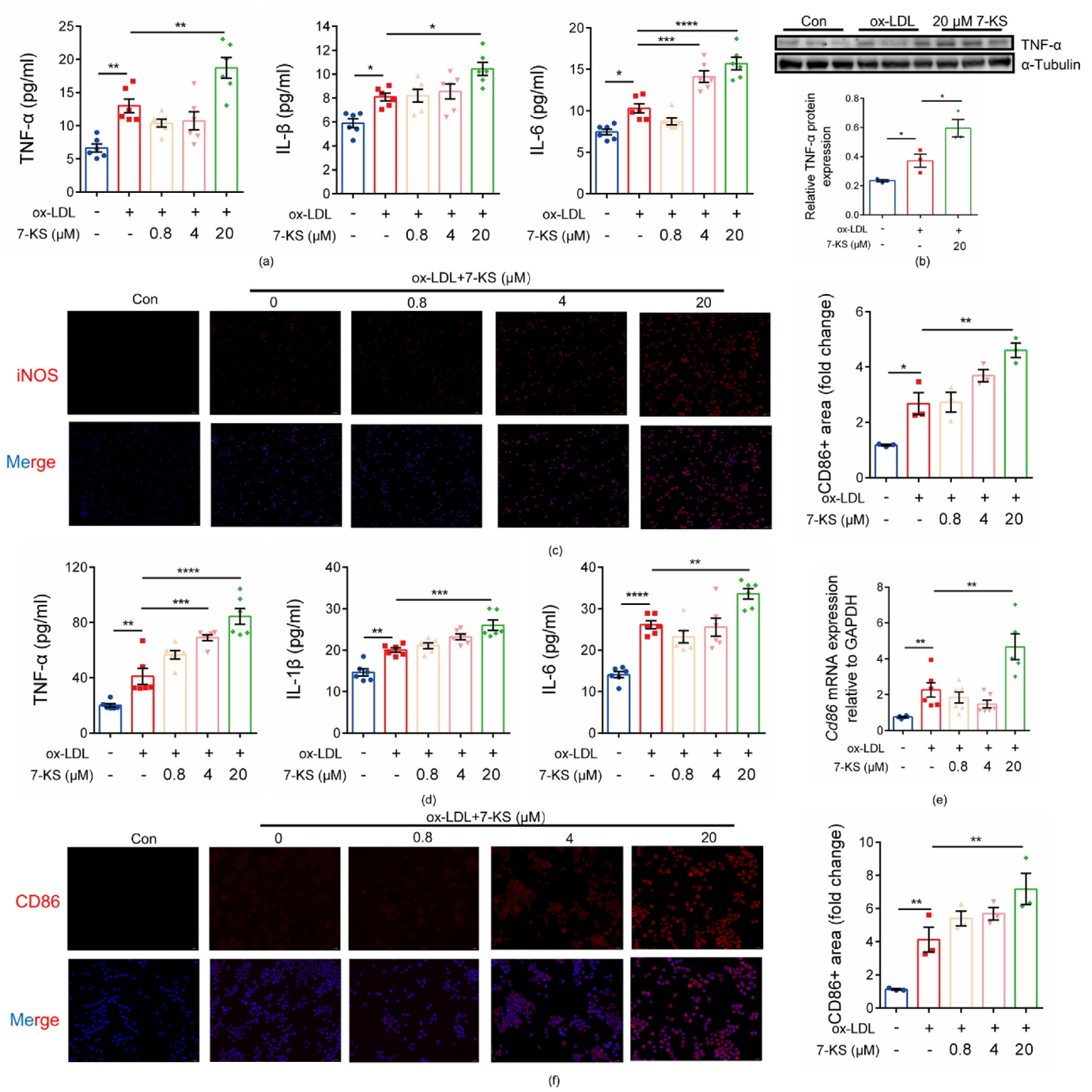

Fig. 4. 7-KS facilitated ox-LDL-induced activation and polarization of macrophages. (a–c) Isolated BMDMs were stimulated with ox-LDL (90 ng·mL^{-1}) and treated with increasing concentrations (mmol·L^{-1}) of 7-KS for 24 h. (a) Culture supernatants from the designated treatment groups were assayed for TNF-α, IL-1β, and IL-6 levels (n = 6). (b) Western blotting was employed to assess TNF-α expression (n = 3). (c) iNOS expression visualized through immunofluorescence imaging (n = 3). (d–f) RAW264.7 cells were stimulated with ox-LDL (90 ng·mL^{-1}) and treated with increasing concentrations (mmol·L^{-1}) of 7-KS for 24 h. (d) Culture supernatants from the designated treatment groups were assayed for TNF-α, IL-1β, and IL-6 levels (n = 6). (e) qRT-PCR analysis revealed *Cd86* mRNA expression levels normalized to *Gapdh* (n = 6). (f) CD86 expression visualized through immunofluorescence imaging (n = 3). Data are expressed as mean ± SEM. Statistical analyses were conducted via one-way ANOVA with Dunnett's *post hoc* comparisons.

To ascertain whether the pro-inflammatory effect of 7-KS is TLR4-IRF5 pathway-dependent, we pre-treated BMDM and RAW264.7 cells with TLR4-IN-C34 and YE6144 (specific inhibitors of TLR4 and IRF5, respectively). TLR4-IN-C34 is reported to inhibit macrophage TLR4 expression *in vitro* [38]. In monocytes exposed to the TLR7 and TLR8 ligand R-848, YE6144 (a small-molecule compound) demonstrated substantial inhibition of IRF5 nuclear translocation [39]. In ox-LDL-induced RAW264.7 macrophages, the results showed that TLR4-IN-C34 and YE6144 abolished 7-KS promotion of inflammatory cytokine production (Fig. 5(g)). In addition, immunofluorescent staining of IRF5 demonstrated that 7-KS treatment promoted the translocation of IRF5 into the nucleus in ox-LDL stimulated BMDM and RAW264.7 macrophages, in agreement with the previous WB results (Figs. 5(c) and (f)). Moreover, inhibition of TLR4 and IRF5 significantly decreased the nuclear translocation of IRF5, which explained that inhibitor treatment

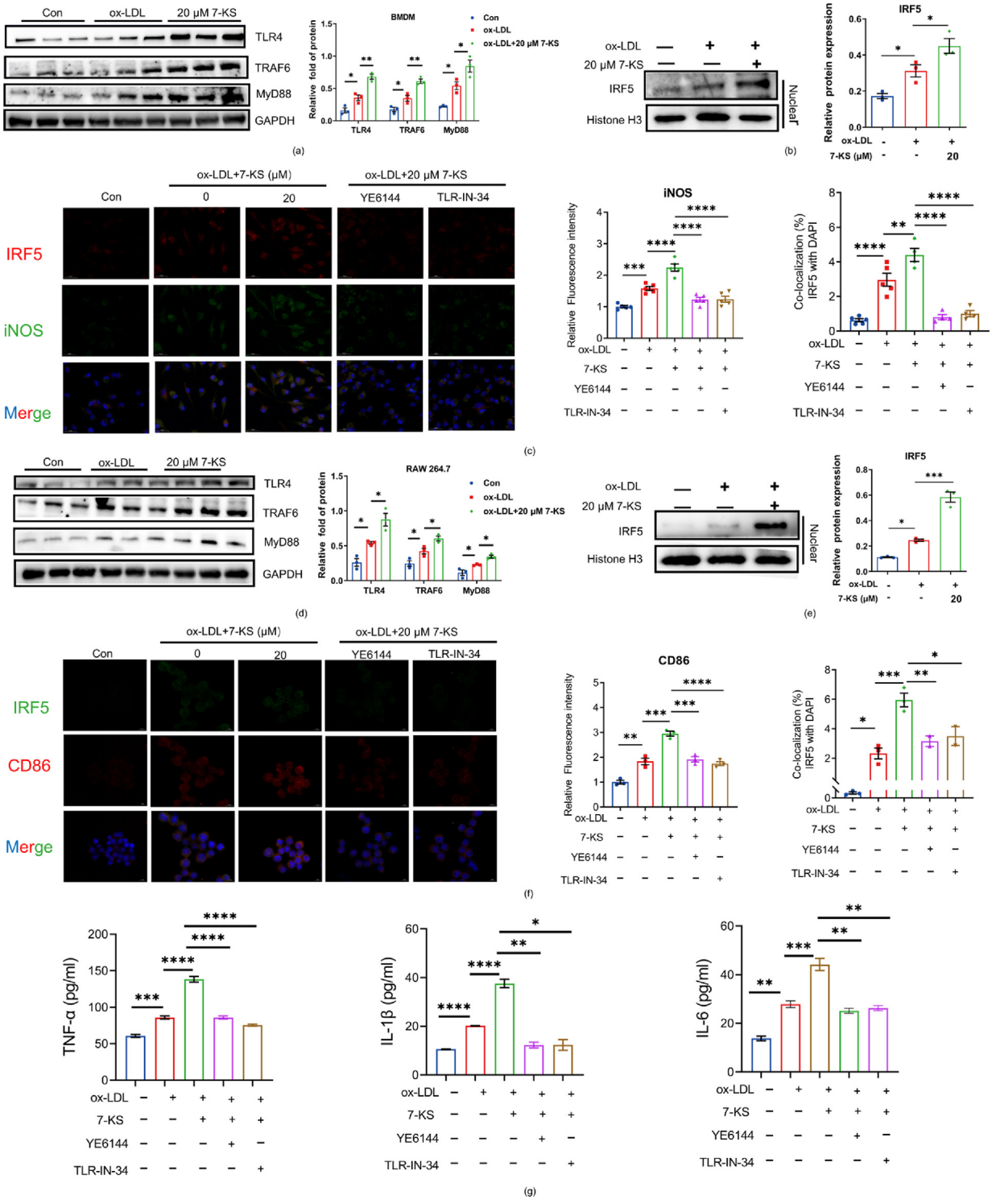

Fig. 5. 7-KS upregulated M1-skewing in a TLR4/IRF5-Dependent Manner. (a–c) BMDM and (d–g) RAW 264.7 cells were pretreated with TLR4-IN-C34 (10 μmol·L^{-1}) and YE6144 (3 μmol·L^{-1}) for 30 min, and then 20 μmol·L^{-1} 7-KS and 90 μg·ml^{-1} ox-LDL was supplemented into the culture medium for 24 h. (a, d) Expression of TLR4, TRAF6 and MyD88 were assessed by immunoblotting (n = 3). (b, e) The nuclear translocation of IRF5 (n = 3). (c) IRF5 and iNOS expression visualized through immunofluorescence imaging. The expression of iNOS and the nuclear shift of IRF5 were quantified (n = 5). (f) IRF5 and iNOS expression visualized through immunofluorescence imaging. The expression of CD86 and the nuclear shift of IRF5 were quantified (n = 3). (g) Culture supernatants from the designated treatment groups were assayed for TNF-α, IL-1β, and IL-6 levels. Data are expressed as mean ± SEM. Statistical analyses were conducted via one-way ANOVA with Dunnett's *post hoc* comparisons.

decreased the pro-inflammatory effect of 7-KS (Figs. 5(c) and (f)). In addition, inhibition of TLR4 and IRF5 reversed the M1 skewing effect of 7-KS. Collectively, these findings suggest that the TLR4-IRF5 axis played a mediating role in the pro-inflammatory effects of 7-KS and promotion of macrophage polarization toward the M1 phenotype.

3.6. Identification of a POP-associated proinflammatory immune niche in community scRNA-seq datasets

Subsequently, we focused on evaluating whether POP-associated M1-like macrophages are also characteristic in human AS. We conducted an analysis of publicly accessible scRNA-seq

data from human arteries using four available community datasets. After quality control, 73 971 cells (normal group: 36 782; patient group: 37 191) were retained for downstream analytical workflows (Fig. S6(a) in Appendix A). Using the Seurat platform workflow, we identified a total of 12 cell clusters (Fig. 6(a)). We successfully mitigated batch effects, as evidenced by the overlap of samples post-integration; variations in cellularity between groups were apparent (Fig. 6(b) and Fig. S6(b) in Appendix A). According to the previously published paper corresponding to the dataset and human aortic cell-specific markers, 12 cell clusters were identified as nine major cell types, including B cells, ECs, fibroblasts, macrophages, mast cells, monocytes, neurons, SMCs, T cells (Fig. 6(b); Table S6 in Appendix A). Subsequently, we computed the relative cellular abundance based on the identified cell types. This revealed an elevated proportion of immune subsets and a reduced fraction of structural components such as fibroblasts and endothelial cells within the lesion (Fig. S6(c) in Appendix A). This finding may be due to the scRNA-seq data in the Patient group was sequenced from $CD45^+$ cells. GO and KEGG enrichment analysis showed that the inflammatory response and toll-like receptor signaling pathways were significantly enriched in the patient group (Figs. S6(d)–(e) in Appendix A). Predictably, differential gene analysis showed that the TLR4 and IRF5 genes exhibited pronounced upregulation in the patient group (Fig. S6(f) in Appendix A).

Next, we investigated whether an equivalent of the POP-associated pathogenic immune niche exists in human AS by performing a comprehensive analysis of macrophage re-clustering. Based on the differences in cluster-specific expression profiles (Table S7 in Appendix A), we distinguished a total of eight subclusters and six subtypes (Fig. 6(c)). Given the previous results from our own scRNA-seq data, we next focused on differences in macrophages, with the normal and patient group including 6379 and 9869 macrophages, respectively. In agreement with previous studies, inflammatory macrophages present in these human plaques exhibited common genes associated with inflammation, such as *Nlrp3*, *IL1B*, *Ccl3*, *CXCL5*, *CCL7*, and *NFKBID*. IFN-responsive macrophages, characterized by high expression of interferon response genes (including *IFI6*, *XAF1*, *IFIT2*, *IFI44L*, and *ISG15*), and Res-like macrophages, with high expression of *F13a1* and *Lyve1*, are consistent with the identification of markers in our scRNA-seq data. We identified a minor macrophage cluster derived from SMCs that expressed *TAGLN*, *ACAT2*, as well as an $APOE^+$ macrophage cluster with a transcriptional signature of *APOE*, *APOC1*. Surprisingly, we also identified mast cells expressing the classical markers *TPSB2*, *CPA3*, *TPSAB1*, and *JCHAIN* (Fig. 6(d)). Compared to the normal group, inflammatory macrophages were significantly increased in AS patients, with a percentage rise from 0.27% to 41.6% (Fig. 6(e)). From another perspective, the abundance of inflammatory macrophages was extremely low in the normal group and very high in the patient group, which is similar to the findings in the datasets we used (GSE213740 and GSE234077), in which inflammatory macrophages accounted for 0.18% and 72% of total macrophages, respectively.

To identify phenotypic differences among inflammatory macrophages, we conducted GSEA analysis on the DEGs observed in each group, unveiling specific activated signaling pathways. GSEA results indicated that inflammatory response and the toll-like receptor signaling pathway showed significant up-regulation in inflammatory macrophages of the patient group, consistent with the pathways enriched in POP-associated M1-like macrophages (Figs. 6(f)–(g)). Surprisingly, we also found MyD88-dependent toll-like receptor pathway was significantly activated in the patient group, consistent with our cell experiments (Fig. 6(h)). To investigate transcriptional dynamics underlying macrophage phenotypic transitions, Monocle3 analysis was applied to macrophage subpopulations. We found that the inflammatory macrophage was localized at the end of the pseudotime, consistent with our single-cell results showing that M1-like macrophages were also at the end of the pseudotime. In addition, we found that the previous state of the inflammatory macrophage was the $ApoE^+$ macrophage (Fig. 6(i)), consistent with a recent study suggesting that lipid-associated macrophages transition to inflammatory macrophages [23]. Surprisingly, we also found that TLR4-IRF5 axis-related genes (TLR4 and IRF5) demonstrated increasing activation across the pseudotemporal trajectory of pro-inflammatory macrophage maturation (Fig. 6(j)).

To further explore potential transcription factor regulators in human plaque macrophages with similar opening characteristics to POP-associated macrophage transcription factors, we employed the SCENIC algorithm to discern activated transcriptional factors (TFs) in inflammatory macrophages. NFKB2, IRF8, and IRF5, characteristic regulators of inflammatory macrophages, are involved in inflammatory regulation (Fig. 6(l)). In particular, we found that IRF5 activity was enhanced in the patient group (Fig. 6(m)). Further comparison of the transcriptional activity of IRF5 within inflammatory macrophages showed that IRF5 was overwhelmingly activated in inflammatory macrophages from the patient group. These results suggest that inflammatory macrophages in human atherosclerotic plaques also share the molecular signature of M1-like macrophages associated with POPs.

4. Discussion

Vascular tissues exhibit significant heterogeneity, and there is an inextricable link between changes in the molecular traits of vascular cells and the development of AS. Hence, gaining a deeper comprehension of the mechanisms linking inflammation and AS at the single-cell level is imperative to identifying new therapeutic approaches aimed at mitigating the residual risk of cardiovascular events. Herein, we analyzed scRNA-seq data and unveiled the impact of POPs on aortic cellular heterogeneity within atherosclerotic murine models. Our findings revealed that myeloid cells potentially contribute to the recruitment of other cells in the plaque microenvironment. Due to the crucial role of myeloid cells in AS, we conducted further studies and observed that POPs increased the number of M1-like macrophages in myeloid cells. Gene enrichment analysis showed that M1-like macrophages in the POP group were significantly enriched for the inflammatory response and Toll-like receptor signaling pathways. Concurrently, we also found that the regulon activity of the transcription factor IRF5 was greater in macrophages from the POP group. In addition, we validated that POPs enhanced proinflammatory M1 skewing through the TLR4-IRF5 inflammatory signaling pathway in BMDM and RAW264.7 cells. Further, we found that the pro-inflammatory effects of POPs and subsequent fostering of M1 polarization were nearly abolished after treatment of macrophages with TLR4 and IRF5 inhibitors. Analysis of publicly accessible scRNA-seq data from human normal and advanced arterial plaques validated the existence of this pro-inflammatory immune niche, which is characterized by elevated enrichment of the inflammatory response and Toll-like receptor signaling pathways.

The application of recent revolutionary advances in scRNA-seq technologies to human and mouse atherosclerotic lesions has enabled cell delineation at ultra-high resolution, leading to breakthroughs in identifying critical cellular subsets and molecular events that underlie the homeostatic and disease-associated stages involved in AS [23,25,40]. POPs are thought to be pro-atherosclerotic due to their elevated levels in the bloodstream of AS patients [11]. Our prior investigation delved into the impact of dietary POPs on AS using liver proteomics and lipidomics [41].

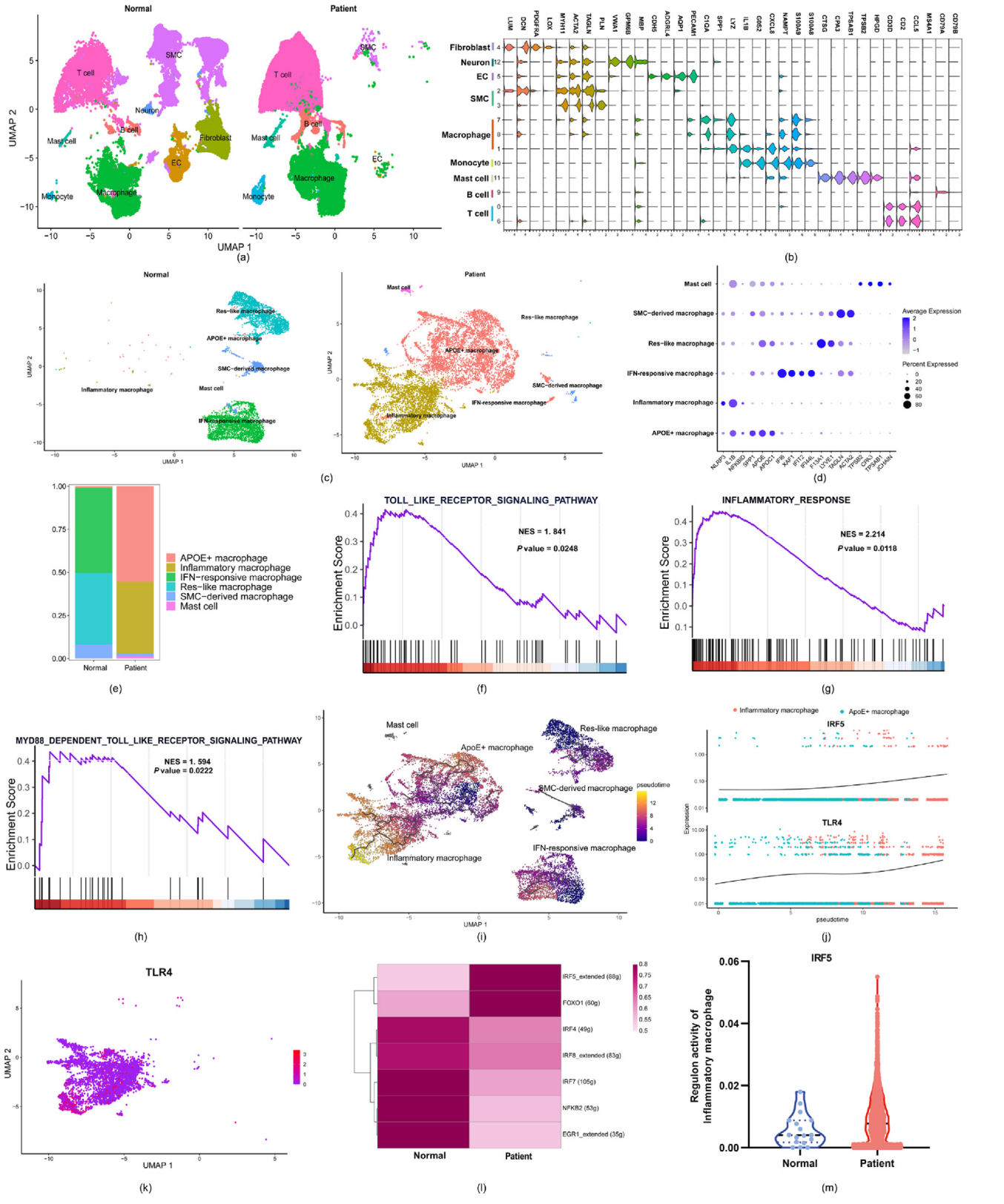

Fig. 6. Validation of the POP-associated pro-inflammatory immune niche in community scRNA-seq datasets. (a) UMAP visualization displayed 13 subclusters. (b) Lineage-specific expression of well-characterized marker genes within individual clusters. (c) The UMAP projection of macrophage subclusters in normal and patient groups. (d) Dot plot of endothelial cell, myeloid cell, fibroblast cell, lymphocyte, SMC, and markers. (e) Stacked bar plot illustrating cluster distribution across normal and patient groups. (f–h) GSEA enrichment profile demonstrated marked enrichment of selected pathways in inflammatory macrophages in the patient group compared with normal group, including (f) toll-like receptor signaling pathway, (g) inflammatory response, and (h) Myd88 dependent toll-like receptor signaling pathway. NES refers to normalized enrichment score. (i) Pseudotemporal trajectories derived by Monocle3 following macrophage reclustering. (j) Trace-plots of IRF5 and TLR4 gene expression levels along the pseudotime. (k) TLR4 expression in inflammatory macrophages. (l) Heatmap of active transcriptional factors (TFs) predicted by SCENIC. (m) Regulon activity of IRF5 in inflammatory macrophages.

However, current evidence suggests the precise mechanisms by which POP promotes AS have yet to be drawn. Prior investigations have predominantly emphasized alterations in cholesterol levels, inflammatory markers, or plaque size in the aorta, with limited attention given to cellular heterogeneity associated with AS. Our study of AS in POP-treated mice constructed a single-cell resolution transcriptional map of the aorta. Within the transcriptional landscape of aortic cells, established cellular subpopulations were identified, including fibroblasts, myeloid cells, lymphocytes, SMCs, and endothelial cells. Analysis of the intercellular communication network revealed that myeloid cells may play a crucial role in coordinating the recruitment of other vascular cells in the plaque microenvironment. Given the substantial impact of POPs on myeloid cells and their pivotal role in AS pathogenesis, we investigated the heterogeneity of myeloid cells. We categorized myeloid cells into five distinct subsets: tissue-resident like macrophages, monocytes, antigen-presentation macrophages, and M1-like macrophages. Gene enrichment analysis results suggest that M1-like macrophages in the POP group were more likely involved in the inflammatory response and toll-like receptor signaling pathway than in the Con group. Predictably, lipoprotein-related activities such as lipoprotein activity and the structure of other lipoproteins were also significantly enriched in the POP group. Therefore, changes in M1-like macrophages in the POP group suggest that M1-like macrophages may be the key cell type regulating the proinflammatory effect of POPs.

The unique functions and developmental characteristics of arterial macrophages are evident, showcasing their adaptability within the diverse surroundings of atherosclerotic plaques. This adaptability underscores the varied nature of these plaques, an aspect that is gaining greater recognition [42]. Various stimuli (e.g., oxidized lipids, TLR ligands) exposed to the plaque microenvironment polarize plaque macrophages toward the pro-inflammatory M1 phenotype, which serves as a critical role in orchestrating AS by initiating and accelerating inflammatory responses away from the anti-inflammatory M2 phenotype [43]. ScRNA-seq has been used to characterize the cellular heterogeneity of macrophages in murine and human atheroma plaques. The TLR4-MyD88 signaling axis recognizes oxidized lipoproteins in experimental models, amplifying foam cell generation and atherogenic progression [44]. In our scRNA-seq results, POP treatment significantly elevated the abundance of M1-like macrophages. Interestingly, we also elucidated the pivotal effect of TLR4 signaling in POP-treated macrophages. We then performed RNA velocity analysis using scVelo to determine the cellular fate of macrophages. Results revealed reconstitution of M1-like macrophages and showed that the top-ranked dynamic driver gene for M1-like macrophages was *Il1r1*. This suggests a progressive enhancement of cellular inflammation along the pseudotime axis. A previous study demonstrated that MyD88-dependent TLR/IL-1R signaling drives inflammatory activation in human AS cell isolates [45]. These findings suggest that a noteworthy surplus of M1 macrophages in the POP group compared to the Con group may be ascribed to the activation of the TLR4-Myd88 signaling pathway, which ultimately skewed macrophages toward the M1 phenotype.

To identify candidate transcriptional regulators downstream of TLR4, we employed pySCENIC. Results showed that the transcriptional factor IRF5 significantly increased the activity of M1 macrophages after POP treatment. The IRF family is pivotal to M1/M2 phenotypic switching. Specifically, IRF4 and IRF3 showed preferential links to M2 polarization, while IRF8, IRF5, and IRF1 demonstrated connections to M1 polarization [46]. Notably, innate immune signaling through the TLR4–IRF5 axis has been implicated in inducing systemic sclerotic phenotypes across various cell types [35]. When TLRs are activated, IRF5 is responsible for upregulating pro-inflammatory mediators, including IL-6, IL-12, and TNF-α, mediated through MyD88-dependent pathway activation in macrophages [36]. Therefore, TLR4-mediated IRF5 activation may contribute to POP-induced skewing of macrophages toward the M1 phenotype and promotion of proinflammatory responses. To validate this hypothesis, we stimulated BMDM and RAW264.7 cells with ox-LDL. Consistent with previous studies, ox-LDL promoted macrophage inflammation and M1 polarization, and these effects were aggravated by 7-KS treatment. Further, we observed that 7-KS treatment increased IRF5 activity by enhancing IRF5 nuclear translocation and increasing IL-1β, IL-6, and TNF-α expression in macrophages. Furthermore, in 7-KS treated macrophages, pharmacological inhibitors of TLR4 and IRF5 (TLR4-IN-C34 and YE6144) significantly blocked entry of IRF5 into the nucleus and secretion of inflammatory factors. These data confirmed that 7-KS accelerated AS progression by contributing to macrophage M1 polarization and promoting inflammatory processes through activation of the TLR4–IRF5 pathway. Collectively, the TLR–IRF5 axis was delineated as a critical regulator of plaque inflammation during atherosclerosis, serving as a central driver of vascular inflammatory development.

Although the biology of the TLR4–IRF5 pathway is well established in mouse and cell models, its specific role in human AS remains relatively unclear. TLR4 expression has been found to be upregulated within human atherosclerotic lesions [47], while other molecular and functional characteristics of these macrophages have not been elucidated. Therefore, we analyzed existing public scRNA-seq datasets from human arteries to establish whether POP-associated M1-like macrophages are a characteristic feature of human AS. After annotation, we identified cell populations similar to those reported in the original paper. Subsequently, macrophages were further analyzed for re-clustering. As expected, the Patient group demonstrated a significant elevation in inflammatory macrophage abundance compared to healthy controls. It is noteworthy that neither our scRNA-seq data nor publicly available scRNA-seq data have demonstrated an anti-inflammatory (M2-like) phenotype [5,48,49]. This finding aligns with results from other scRNA-seq analyses in murine and human atherosclerotic lesions, suggesting the population likely reflects either undetectably rare or nonexistent cell subsets within plaques. Meanwhile, this observation aligns with M1 macrophage predominance relative to M2 subsets in AS progression [50]. To further validate the existence of macrophage, a molecular signature similar to that induced by POPs, we revealed the key contribution of MyD88-dependent toll-like receptor pathway signaling and IRF5 in inflammatory macrophages from the Patient group using GSEA and SCENIC analysis. Results suggest that inflammatory signaling contributes to the transition of macrophages toward a proinflammatory state, providing vital clues for the development of novel AS treatments.

Our findings are subject to several limitations. Primarily, we did not thoroughly investigate the effects of TLR4 and IRF5 in the context of ApoE$^{-/-}$ macrophage-specific knockdown using *in vivo* models. It is imperative that future studies address this gap in the research. Second, macrophage polarization may vary significantly across atherosclerotic plaques depending on their vascular origins or stability stages [51]. Hence, the findings from the heterogeneous human ascending aorta and carotid artery samples provided here may not be universally applicable to all atherosclerotic plaques. Finally, the GEO dataset that we used for histological validation of our bench study findings from the artery specimens lacked corresponding tissue samples.

5. Conclusions

In conclusion, our study elucidated the cell-specific profiles of ApoE$^{-/-}$ mouse aortas and a POP-linked pro-inflammatory immune

microenvironment through single-cell resolution profiling. This offers critical insights regarding the biological function of food components. We also delineated the transcriptional profile of M1-like macrophages exhibiting pathological cellular traits and identified TLR4 signaling and IRF5 as key drivers of M1-like macrophage induction in the POP group. Further experimental verification revealed that the TLR4–IRF5 axis was necessary for the proinflammatory effects and induction of M1 polarization by 7-KS is indispensable in ox-LDL stimulated BMDM and RAW 264.7 cells for the proinflammatory and M1 polarization of 7-KS, the most abundant POP in foods. Delving deeper into the scRNA-seq data of 19 human artery specimens, we have provided a comprehensive reference atlas for future research on human atherosclerotic syndromes. We have also corroborated the prevalence of a pro-inflammatory immune niche exhibiting molecular features associated with POPs, underscoring the pivotal role of this pro-inflammatory immune niche in the essential cellular and molecular processes leading to atherosclerotic plaques.

CRediT authorship contribution statement

Qinjun Zhang: Visualization, Investigation, Conceptualization, Writing – review & editing, Validation, Formal analysis, Writing – original draft, Methodology, Data curation. **Weisu Huang:** Investigation, Writing – original draft, Visualization. **Cheng Chen:** Visualization. **Jianfu Shen:** Supervision, Project administration. **Baiyi Lu:** Supervision, Conceptualization, Project administration, Writing – review & editing, Funding acquisition. **Peiwu Li:** Supervision, Project administration, Writing – review & editing.

Declaration of competing interest

The authors declare that they have no known competing financial interests or personal relationships that could have appeared to influence the work reported in this paper.

Acknowledgments

This study was supported by the "Pioneer" and "Leading Goose" Research and Development Programs of Zhejiang Province (2025C01100) and Zhejiang Provincial Natural Science Foundation of China (LY24C200003 and LD21C200001) and the National Natural Science Foundation of China (32072179).

Appendix A. Supplementary data

Supplementary data to this article can be found online at https://doi.org/10.1016/j.eng.2025.07.021.

References

[1] Tsao CW, Aday AW, Almarzooq ZI, Anderson CA, Arora P, Avery CL, et al. Heart disease and stroke statistics—2023 update: a report from the American Heart Association. Circulation 2023;147(8):e93–e621.
[2] Escaned J, Davies J. Physiological assessment of coronary stenoses and the microcirculation (No. 25560). London: Springer London; 2017.
[3] Ridker PM, Everett BM, Thuren T, MacFadyen JG, Chang WH, Ballantyne C, et al. Antiinflammatory therapy with canakinumab for atherosclerotic disease. N Engl J Med 2017;377(12):1119–31.
[4] Tardif JC, Kouz S, Waters DD, Bertrand OF, Diaz R, Maggioni AP, et al. Efficacy and safety of low-dose colchicine after myocardial infarction. N Engl J Med 2019;381(26):2497–505.
[5] Depuydt MA, Prange KH, Slenders L, Örd T, Elbersen D, Boltjes A, et al. Microanatomy of the human atherosclerotic plaque by single-cell transcriptomics. Circ Res 2020;127(11):1437–55.
[6] Zernecke A, Winkels H, Cochain C, Williams JW, Wolf D, Soehnlein O, et al. Meta-analysis of leukocyte diversity in atherosclerotic mouse aortas. Circ Res 2020;127(3):402–26.
[7] Cochain C, Vafadarnejad E, Arampatzi P, Pelisek J, Winkels H, Ley K, et al. Single-cell RNA-seq reveals the transcriptional landscape and heterogeneity of aortic macrophages in murine atherosclerosis. Circ Res 2018;122(12):1661–74.
[8] Mutemberezi V, Guillemot-Legris O, Muccioli GG. Oxysterols: from cholesterol metabolites to key mediators. Prog Lipid Res 2016;64:152–69.
[9] O'Callaghan Y, McCarthy FO, O'Brien NM. Recent advances in phytosterol oxidation products. Biochem Biophys Res Commun 2014;446(3):786–91.
[10] Gylling H, Plat J, Turley S, Ginsberg HN, Ellegård L, Jessup W, et al. Plant sterols and plant stanols in the management of dyslipidaemia and prevention of cardiovascular disease. Atherosclerosis 2014;232(2):346–60.
[11] Barriuso B, Ansorena D, Astiasarán I. Oxysterols formation: a review of a multifactorial process. J Steroid Biochem Mol Biol 2017;169:39–45.
[12] Fuhrmann A, Weingärtner O, Meyer S, Cremers B, Seiler-Mußler S, Schött HF, et al. Plasma levels of the oxyphytosterol 7α-hydroxycampesterol are associated with cardiovascular events. Atherosclerosis 2018;279:17–22.
[13] Pordal AH, Hajmiresmail SJ, Assadpoor-Piranfar M, Hedayati M, Ajami M. Plasma oxysterol level in patients with coronary artery stenosis and its changes in response to the treatment with atorvastatin. Med J Islam Repub Iran 2015;29:192.
[14] Gao J, Chen S, Zhang L, Cheng B, Xu A, Wu L, et al. Evaluation of cytotoxic and apoptotic effects of individual and mixed 7-ketophytosterol oxides on human intestinal carcinoma cells. J Agric Food Chem 2015;63(3):1035–41.
[15] Ryan E, Chopra J, McCarthy F, Maguire AR, O'Brien NM. Qualitative and quantitative comparison of the cytotoxic and apoptotic potential of phytosterol oxidation products with their corresponding cholesterol oxidation products. Br J Nutr 2005;94(3):443–51.
[16] Barut Z, Aslan M, Çırçırlı B, Çeker T, Yılmaz Ç. Antiproliferative effect of 7-ketositosterol in breast and liver cancer cells: possible impact on ceramide, extracellular signal-regulated kinases, and nuclear factor Kappa B signaling pathways. Pharmaceuticals 2024;17(7):860.
[17] O'Callaghan YC, Foley DA, O'Connell NM, McCarthy FO, Maguire AR, O'brien NM. Cytotoxic and apoptotic effects of the oxidized derivatives of stigmasterol in the U937 human monocytic cell line. J Agric Food Chem 2010;58(19):10793–8.
[18] Liang YT, Wong WT, Guan L, Tian XY, Ma KY, Huang Y, et al. Effect of phytosterols and their oxidation products on lipoprotein profiles and vascular function in hamster fed a high cholesterol diet. Atherosclerosis 2011;219(1):124–33.
[19] Oligschlaeger Y, Houben T, Jeurissen MLJ, Bitorina AV, Konings M, Baumgartner S, et al. Exogenously added oxyphytosterols do not affect macrophage-mediated inflammatory responses. Lipids 2018;53(4):457–62.
[20] Yan J. 7-Ketositosterol in ultra-processed foods aggravates colitis by gut dysbiosis induced-PDLIM3 activation. Gut 2024;73:A133–4.
[21] Vanmierlo T, Husche C, Schött HF, Pettersson H, Lütjohann D. Plant sterol oxidation products–analogs to cholesterol oxidation products from plant origin? Biochimie 2013;95(3):464–72.
[22] Zhang B, Zeng K, Guan RC, Jiang HQ, Qiang YJ, Zhang Q, et al. Single-cell RNA-Seq analysis reveals macrophages are involved in the pathogenesis of human sporadic acute type A aortic dissection. Biomolecules 2023;13(2):399.
[23] Dib L, Koneva LA, Edsfeldt A, Zurke YX, Sun J, Nitulescu M, et al. Lipid-associated macrophages transition to an inflammatory state in human atherosclerosis, increasing the risk of cerebrovascular complications. Nat Cardiovasc Res 2023;2(7):656–72.
[24] Slysz J, Sinha A, DeBerge M, Singh S, Avgousti H, Lee I, et al. Single-cell profiling reveals inflammatory polarization of human carotid versus femoral plaque leukocytes. JCI Insight 2023;8(17):e171359.
[25] Liu X, Chen W, Zhu G, Yang H, Li W, Luo M, et al. Single-cell RNA sequencing identifies an *Il1rn*$^{+}$/*Trem1*$^{+}$ macrophage subpopulation as a cellular target for mitigating the progression of thoracic aortic aneurysm and dissection. Cell Discov 2022;8(1):11.
[26] Yu L, Zhang J, Gao A, Zhang M, Wang Z, Yu F, et al. An intersegmental single-cell profile reveals aortic heterogeneity and identifies a novel Malat1^{+} vascular smooth muscle subtype involved in abdominal aortic aneurysm formation. Signal Transduct Target Ther 2022;7(1):125.
[27] Siegmund D, Wajant H. TNF and TNF receptors as therapeutic targets for rheumatic diseases and beyond. Nat Rev Rheumatol 2023;19(9):576–91.
[28] Dick SA, Macklin JA, Nejat S, Momen A, Clemente-Casares X, Althagafi MG, et al. Self-renewing resident cardiac macrophages limit adverse remodeling following myocardial infarction. Nat Immunol 2019;20(1):29–39.
[29] Narasimhan PB, Marcovecchio P, Hamers AA, Hedrick CC. Nonclassical monocytes in health and disease. Annu Rev Immunol 2019;37:439–56.
[30] Zhang K, Wang Y, Chen S, Mao J, Jin Y, Ye H, et al. TREM2hi resident macrophages protect the septic heart by maintaining cardiomyocyte homeostasis. Nat Metab 2023;5(1):129–46.
[31] Sun X, Zhou L, Wang Y, Deng G, Cao X, Ke B, et al. Single-cell analyses reveal cannabidiol rewires tumor microenvironment via inhibiting alternative activation of macrophage and synergizes with anti-PD-1 in colon cancer. J Pharm Anal 2023;13(7):726–44.
[32] La Manno G, Soldatov R, Zeisel A, Braun E, Hochgerner H, Petukhov V, et al. RNA velocity of single cells. Nature 2018;560(7719):494–8.
[33] Hennessy EJ, Parker AE, O'neill LA. Targeting toll-like receptors: emerging therapeutics? Nat Rev Drug Discov 2010;9(4):293–307.
[34] Huang R, Hu Z, Chen X, Cao Y, Li H, Zhang H, et al. The transcription factor SUB1 is a master regulator of the macrophage TLR response in atherosclerosis. Adv Sci 2021;8(19):2004162.
[35] Saigusa R, Asano Y, Taniguchi T, Yamashita T, Ichimura Y, Takahashi T, et al. Multifaceted contribution of the TLR4-activated IRF5 transcription factor in systemic sclerosis. Proc Natl Acad Sci USA 2015;112(49):15136–41.

[36] Takaoka A, Yanai H, Kondo S, Duncan G, Negishi H, Mizutani T, et al. Integral role of IRF-5 in the gene induction programme activated by toll-like receptors. Nature 2005;434(7030):243–9.
[37] Ban T, Sato GR, Tamura T. Regulation and role of the transcription factor IRF5 in innate immune responses and systemic lupus erythematosus. Int Immunol 2018;30(11):529–36.
[38] Neal MD, Jia H, Eyer B, Good M, Guerriero CJ, Sodhi CP, et al. Discovery and validation of a new class of small molecule toll-like receptor 4 (TLR4) inhibitors. PLoS One 2013;8(6):e65779.
[39] Ban T, Kikuchi M, Sato GR, Manabe A, Tagata N, Harita K, et al. Genetic and chemical inhibition of IRF5 suppresses pre-existing mouse lupus-like disease. Nat Commun 2021;12(1):4379.
[40] Wang Z, Zhang X, Lu S, Zhang C, Ma Z, Su R, et al. Pairing of single-cell RNA analysis and T cell antigen receptor profiling indicates breakdown of T cell tolerance checkpoints in atherosclerosis. Nat Cardiovasc Res 2023;2(3):290–306.
[41] Wang M, Liu Y, Zhao T, Xiao F, Yang X, Lu B. Dietary sterols and sterol oxidation products on atherosclerosis: an insight provided by liver proteomic and lipidomic. Mol Nutr Food Res 2021;65(20):2100516.
[42] Mori H, Finn AV, Kolodgie FD, Davis HR, Joner M, Virmani R. Atherogenesis: the development of stable and unstable plaques. In: Escaned J, Davies J, editors. Physiological assessment of coronary stenoses and the microcirculation. Berlin: Springer; 2017. p. 21–37.
[43] Murray PJ, Allen JE, Biswas SK, Fisher EA, Gilroy DW, Goerdt S, et al. Macrophage activation and polarization: nomenclature and experimental guidelines. Immunity 2014;41(1):14–20.
[44] Stewart CR, Stuart LM, Wilkinson K, Van Gils JM, Deng J, Halle A, et al. CD36 ligands promote sterile inflammation through assembly of a toll-like receptor 4 and 6 heterodimer. Nat Immunol 2010;11(2):155–61.
[45] Monaco C, Gregan SM, Navin TJ, Foxwell BM, Davies AH, Feldmann M. Toll-like receptor-2 mediates inflammation and matrix degradation in human atherosclerosis. Circulation 2009;120(24):2462–9.
[46] Chistiakov DA, Myasoedova VA, Revin VV, Orekhov AN, Bobryshev YV. The impact of interferon-regulatory factors to macrophage differentiation and polarization into M1 and M2. Immunobiology 2018;223(1):101–11.
[47] Xu XH, Shah PK, Faure E, Equils O, Thomas L, Fishbein MC, et al. Toll-like receptor-4 is expressed by macrophages in murine and human lipid-rich atherosclerotic plaques and upregulated by oxidized LDL. Circulation 2001;104(25):3103–8.
[48] Winkels H, Ehinger E, Vassallo M, Buscher K, Dinh HQ, Kobiyama K, et al. Atlas of the immune cell repertoire in mouse atherosclerosis defined by single-cell RNA-sequencing and mass cytometry. Circ Res 2018;122(12):1675–88.
[49] Fernandez DM, Rahman AH, Fernandez NF, Chudnovskiy A, Amir ED, Amadori L, et al. Single-cell immune landscape of human atherosclerotic plaques. Nat Med 2019;25(10):1576–88.
[50] Basu A, Dvorina N, Baldwin III WM, Mazumder B. High-fat diet-induced GAIT element-mediated translational silencing of mRNAs encoding inflammatory proteins in macrophage protects against atherosclerosis. FASEB J 2020;34(5):6888.
[51] Liu N, Zhang B, Sun Y, Song W, Guo S. Macrophage origin, phenotypic diversity, and modulatory signaling pathways in the atherosclerotic plaque microenvironment. Vessel Plus 2021;5:43.